Chapter 10
Cavitation

Abstract Cavitation is of great technical importance. Nucleated cavities grow and link to form cracks that can cause rupture. During creep, cavities are initiated in the grain boundaries. The nucleation takes place at particles or at subboundary—grain boundary junctions. The main mechanism is believed to be grain boundary sliding (GBS), Chap. 9. According to the double ledge model, cavities are formed when the particles or subboundaries meet other subboundaries. With this assumption quantitative models for cavity nucleation can be derived. They show that the nucleated number of cavities is proportional to the creep strain in good accordance with observations. Cavities can grow by diffusion or by straining. It is important to take into account that cavities cannot grow faster than the surrounding creeping matrix, which is referred to as constrained growth. Otherwise the growth rate can be significantly overestimated. Models both for diffusion and strain controlled growth have been available for a long time. A recently developed model for strain controlled growth is presented based on GBS. It has the advantage that is associated with a well-defined initiation size of cavities and that constrained growth is automatically taken into account, features that some previous strain controlled models miss.

10.1 General

During creep micrometer sized holes are formed in alloys. These holes are called cavities. The presence of cavities is technologically important because the cavities have a strong influence on the final rupture, in particular at low stresses. Quantitative studies of cavitation have mainly been performed in three groups of alloys that will be referred to as Group I, Group II and Group III. Group I consists of fcc alloys: copper, austenitic stainless steels and nickel-base alloys. Group II includes creep resistant low alloy steels typically with a ferritic-bainitic microstructure. Also the classical 12%Cr steel (X20) is included in this group because it shows the same type of behavior. Group III represents the advanced martensitic 9% Cr creep resistant steel. The reason why it is important to distinguish between these groups is that the cavitation occurs in different ways. In Group I, the cavities appear mainly in the

R. Sandström, *Basic Modeling and Theory of Creep of Metallic Materials*, Springer Series in Materials Science 339,
https://doi.org/10.1007/978-3-031-49507-6_10

grain boundaries, and in Group II the cavities are found in the prior austenite grain boundaries. The main location of cavities in Group III is the lath boundaries in the martensite. For a review on earlier work on cavitation during creep, see [1] and for more recent work [2].

Models for the formation and growth of cavities have primarily been developed for Group I and II alloys. The analysis in this chapter will concentrate on these types. Much less is known about the martensitic steels in Group III in spite of their extensive use in modern fossil fired power plants. Information about Group III steels will be summarized in Sect. 10.3.

The cavitation in Group I and II can be discussed in the same way, just recalling that when grain boundaries are discussed they are the genuine grain boundaries in Group I but the prior austenite grain boundaries in Group II.

During creep deformation there is some sliding along grain boundaries. Thus, there is a movement between neighboring grains that is called *grain boundary sliding (GBS)*, Chap. 9. The distance that neighboring grains move with respect to each other is referred to as the amount of GBS. According to finite element work, the amount of GBS is proportional to the creep strain. This is further discussed in Chap. 9.

GBS is believed to be essential for cavity formation. If particles are present in the grain boundaries cavities can be created when the boundaries slide. Modeling of initiation of creep cavitation was first made with the help of classical nucleation theory (CNT) [3]. This approach is however associated with several disadvantages. It suggests that cavitation would essentially appear at high stresses, which is in contrast to observations for engineering steels where cavitation is primarily observed at low stresses. CNT tends to give results that appear as a step function in stress and temperature again at variance with observations. With CNT it is very difficult to make quantitative predictions since results are sensitive to the exact values of the chosen parameters. There are many experiments that give that the number of cavities is proportional to the creep strain [4, 5] which is difficult to model with CNT.

With the help of dislocation pile-ups, large stresses can be introduced that could initiate creep cavities [6]. Very large stresses in the GPa range are needed to form cavities in this way. Very long pile-ups are required that are rarely observed in the presence of creep cavities. High stresses can also be generated with the help of a shear crack. Riedel used that approach to model cavity formation with the help of CNT [7]. However, both these types of models have the same problems with the stress dependence as for CNT models in general.

It has been even more challenging to understand how cavities can be created in essentially particle free materials like pure copper. It has been demonstrated that the substructure can act as hard zones in the same way as particles. Lim has shown that subboundaries interacting with a sliding grain boundary can form cavities and that the process is thermodynamically feasible [8]. It is therefore natural to assume that the cavity formation around particles that is experimentally well documented is associated with the interaction with the substructure.

Taking into account the role of GBS and the substructure it can directly be explained why the number of nucleated cavities is proportional to the creep strain for many materials. The proportionality to the strain was first demonstrated by Dyson

[4] and later surveyed in [5]. Although this empirical rule has been known for many years, a basic model was only derived recently based on the so called double ledge principle. In this way the value of the proportionality constant could be derived. This is shown in Sect. 10.4.

Already during the 1950ties, Hull and Rimmer derived a model for growth of cavities based on diffusion control. However, it was found that their model typically exaggerated the growth rate. Dyson realized that the cavities could not grow faster than what the creep rate allows [9]. This is referred to as constrained growth. Although good models for this effect were derived, they still tended to give a too large growth rate. In fact, in models for creep damage development, strain dependent growth is often used in spite of the availability of basic diffusion controlled growth models [10]. A revised constrained cavity growth model has recently been presented, which gives significantly reduced growth rates and solves some of the previous issues. This is analyzed in Sect. 10.5.

After the design life of fossil fired power plants and other high temperature units has expired, almost invariably the plant owners want to extend the service time. Then it is essential to demonstrate that continued operation is safe. The main life controlling factors are related to material properties, not least to creep. Many material properties degrade during service. The determination of the degree of property degradation is referred to as *residual life analysis*, which is a major research area today. Concerning creep properties, the study of cavitation has and is playing a major role in this respect. Neubauer found that the structure of the cavitation changed in components during service [11]. It could be followed by taking replicas on components, which were studied in the laboratory. First a limited number of single cavities appeared in the grain boundaries (category I). Then single cavities were observed in larger numbers (category II). Cavities gradually linked to micro-cracks (shorter than a grain diameter) (category III). Finally macro-cracks appeared (larger than the grain diameter) (category IV). These categories and their interpretation can be found in many versions. Their value is that it typically takes a number of years from category I to II and from II to III. Only for category IV, immediate action in the form of repair or replacement of the component is essential. In this way a system of early warning of serious creep damage was established. It has been extensively used. It has avoided many fatal accidents and saved many lives. Fatal accidents are fortunately rare nowadays.

The use of replication to follow the development of creep damage is the most used traditional method in residual life analysis and also the most successful one. A review of non-destructive methods for residual life analysis can be found in [12]. Welded joints are particularly prone to creep damage, and in particular the fine grained part of the heat affected zone. The Neubauer scheme seems to work well for Group I and Group II materials. However, for the modern martensitic steels in Group III, single cavities in large extent only appear close to rupture and to find cavities that have linked to microcracks is unusual. Early warning of serious creep damage is difficult to get. This will be further discussed in Sect. 10.3.

10.2 Empirical Cavity Nucleation and Growth Models

As mentioned above, the number of cavities formed during creep n_{cav} was early on observed to be approximately proportional to the creep strain ε

$$n_{cav} = B_s \varepsilon \tag{10.1}$$

B_s is a constant. This relation was found to be valid for Group I materials 347 (austenitic stainless steel) and Nimonic 80A (nickel base alloy) and for low alloy steels in Group II 1Cr0.5Mo, 0.5Cr0.5Mo0.25 V, 1Cr1Mo0.25 V and 2.25Cr1Mo as well as 12CrMoV steels [4, 5]. Notice that there is no constant term in Eq. (10.1). The observations show that the formation of cavities starts already at small strains.

Hull and Rimmer formulated a basic expression for diffusion controlled growth of cavities [13]. The equation expresses that the time derivate of the cavity volume is proportional to the grain boundary diffusion coefficient and the applied stress. As pointed out above the resulting growth rate often greatly exceeded the observed values. The situation was much improved when constrained growth was taken into account to ensure that cavity growth rate was not faster than the creep rate. A number of authors derived models for the reduced stress during constrained growth. For example, Rice derived such a model [14].

Cavitation models are extensively used in continuum damage mechanics (CDM) to assess the (remaining) creep life of components. Three of the common approaches in CDM that are supposed to be based on physical constitutive equations are given in [15–17]. A review of the models can be found in [10]. In all three papers an empirical combination of cavity nucleation and growth is used.

$$\dot{\omega}_{cav} = C \dot{\varepsilon}_e \left(\frac{\sigma_1}{\sigma_e} \right)^{\nu} \tag{10.2}$$

where $\dot{\omega}_{cav}$ is the creep damage due to the cavities, $\dot{\varepsilon}_e$ the effective creep rate, σ_1 the maximum principal stress, σ_e the effective stress, and C and ν are constants. Equation (10.2) was originally proposed by Cane [18]. There is no indication in the papers [15–17] why the empirical Eq. (10.2) was chosen and not the basic constrained growth models that were available at the time. There are cases where the growth rate is proportional to the creep strain but that cannot be considered to be a general solution. This will be further discussed in Sect. 10.5.

10.3 Cavitation in 9% Cr Steels

Cavitation has been studied quantitatively to a less extent for modern 9Cr steels (P91, P92) in Group III in comparison to materials in Group I and II. This is surprising considering that they are common materials in pipes and tubes in modern fossil fired

power plants. Much of the data has been collected from ruptured specimens with welds or failed welded components. For a survey, see [19].

In 9Cr steels cavities are primarily formed at lath boundaries, but also at prior austenite grain boundaries. The cavities appear as single units even close to fracture. This should be contrasted to the Group I and II materials where even at fairly low fraction of the rupture life the cavities are arranged in rows at the grain boundaries ("pearls on string"). At higher life fraction the cavities link and form microcracks and then macrocracks. These three later stages are absent in Group III materials. In addition the cavities in Group III materials are observed only very close to the fine grained zone in the HAZ, where the failure takes place (type IV cracking). All these facts make is more difficult to locate the cavitation.

Siefert and Parker [19] made an attempt to estimate the number of cavities n_{cav} as a function of the life fraction t/t_R

$$\frac{n_{cav}}{n_{cavR}} = \left(1 - \frac{t}{t_R}\right)^{\mu_{cav}} \tag{10.3}$$

where n_{cavR} is the number of cavities close to rupture that is estimated to be about 800 cavities per mm^2. μ_{cav} is a constant. For materials with a low creep ductility $\mu_{cav} = 0.5$. Although the majority of casts of P91 has a high ductility, there is a significant fraction where the reduction of area at rupture is less than 20%. μ_{cav} is reduced with increasing ductility, which means that the cavitation appears later in life. This has to be taken into account in residual life time analysis.

It has been found that it is often more difficult to observe cavities metallographically for Group III than for the other Groups. This applies both to replication and direct observation in the lab (Charman, personal communication 2021). It is recommended to use laser microscopy to safely observe the cavities.

In Sects. 10.4 and 10.5 basic models for cavity nucleation and growth are introduced. These models are based on the assumption that the cavities are located at the grain boundaries. Since this is not always the case for Group III materials, the models are not automatically satisfied. Since suitable data for the strain and time dependence of cavitation of 9Cr steels cannot be located, it is not possible to be more specific about the applicability of the models for the Group III materials.

10.4 Basic Model for Cavity Nucleation

10.4.1 Thermodynamic Considerations

In the past a number of mechanisms have been proposed for the formation of creep cavities. One idea is that atomic bonds are ruptured. However, this requires very high stresses and even if such stresses would be initiated they would quickly relax in a creeping material [6]. Another suggestion is that the accumulation of vacancies

can be handled with classical nucleation theory [3]. This gives a very strong stress dependence suggesting that cavities would almost exclusively appear at high stresses [20]. This is at variance with observations since most cavities are formed at low stresses. High stresses can appear at grain boundary ledges, triple points and particles. A common assumption is that cavities are formed by decohesion at particles. High stresses are required in most models. A threshold must be exceeded and an incubation time is required [3, 21]. Contrary to these suggestions, observations demonstrate that cavity nucleation is strain controlled rather than by stress and cavitation is particularly frequent at low stresses as pointed out above. Statements in the literature have also concluded that earlier theories are not successful [22, 23]. These papers also give excellent reviews of earlier work.

New ideas for nucleation mechanisms came from the studies on copper. It is well established that extensive cavitation can take place in copper during creep [24]. It is noticeable that the number of particles is typically so low that they cannot contribute significantly to the cavitation. A model by Lim gave a possible explanation [25]. He assumed that a sliding grain boundary can form cavities where subboundaries reach the boundary. Grain boundary dislocations formed pile ups that exerted sufficient stress on the grain boundary–subboundary intersection that a cavity could be nucleated. He made a thermodynamic analysis of the situation and showed that an energy gain was obtained when a cavity was formed. In his model, the high stress is a result of a stationary creep process and avoids the problem with stress relaxation. The change in free energy during the formation of a cavity can be expressed as

$$\Delta G = -r^3 F_v \sigma_{appl} + r^2 F_s \gamma_s - r^2 F_{GB} \gamma_{GB} - (\Delta G_1 + \Delta G_2 + \Delta G_3) \qquad (10.4)$$

γ_s and γ_{GB} are the surface and grain boundary energies per unit area and

$$F_v = 2\pi/3(2 - 3\cos\alpha + \cos^3\alpha)$$

$$F_s = 4\pi(1 - \cos\alpha)$$

$$F_{GB} = \pi \sin^2\alpha$$

where α is half the tip angle of the cavity. The first term in Eq. (10.4) is the work done by the applied stress. The second and third terms represent the modification in the surface and grain boundary energies when a cavity is formed. The fourth term is the decrease in the strain energy. ΔG_1 is the change in the line energy of the grain boundary dislocations (GBD). ΔG_2 is the interaction energy between the remaining and the consumed GBD. The strain energy ΔG_3 is the reduction of the strain energy of GBDs outside the cavity. Details of the application of Lim's fairly complex model can be found in [26, 27].

Cavitation in copper and austenitic stainless steels has been analyzed with Lim's model. If ΔG in Eq. (10.4) is negative, cavitation can take place. When the applied stress σ_{appl} is raised ΔG becomes more negative and cavitation is more likely. On the

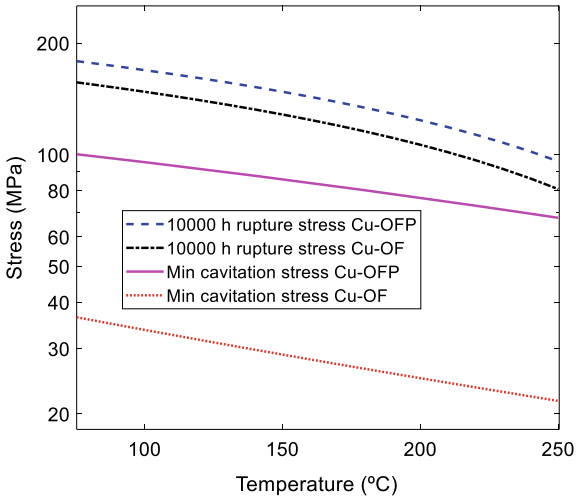

Fig. 10.1 Minimum stress to form cavities at cell boundaries versus temperature for oxygen free pure Cu-OF and phosphorus alloyed copper Cu-OFP. For comparison the stress that gives creep rupture after one year (10000 h) is included. From [28]. Reproduced with the permission of Elsevier

other hand if σ_{appl} is reduced cavitation does not readily occur. This is precisely as expected. When σ_{appl} is below a minimum value ΔG becomes positive and cavitation is no longer possible. This minimum cavitation stress for Cu is shown as a function of temperature in Fig. 10.1. The main temperature dependence is due to the last term in Eq. (10.4).

A comparison is made in Fig. 10.1 to the creep rupture strength for copper for 10000 h. The rupture strength are higher than the minimum cavitation stresses. Since the rupture strength is used in design (with a safety factor), this demonstrates that cavitation at the intersections between subboundaries and grain boundaries is a thermodynamically feasible process.

It is well documented that oxygen free copper Cu-OF can have a much lower creep ductility than the same alloy with 50 wt. ppm P, Cu-OFP [29]. It has therefore been decided to use Cu-OFP but not Cu-OF in copper canisters for disposal of spent nuclear fuel [30]. The origin of the low creep ductility of Cu-OF is the extensive formation of creep cavities [30]. It is evident from Fig. 10.1 that the minimum cavitation stress is much lower for Cu-OF than for Cu-OFP, which explains the difference in creep ductility between the materials, Sect. 13.3.1.

It can also be demonstrated that the minimum cavitation stress is well below the rupture strength for common austenitic stainless steels 304H (18Cr10Ni), 316H (17Cr12Ni2Mo), 321H (18Cr12NiTi), 347H (18Cr12NiNb) [31]. This is illustrated for 347H in Fig. 10.2. The ratio between the rupture strength and the minimum cavitation stress is reduced with increasing temperature, which would suggest that the amount of cavitation would be reduced with increasing temperature contrary to observations. It is likely that Lim's model does not fully give the correct temperature dependence.

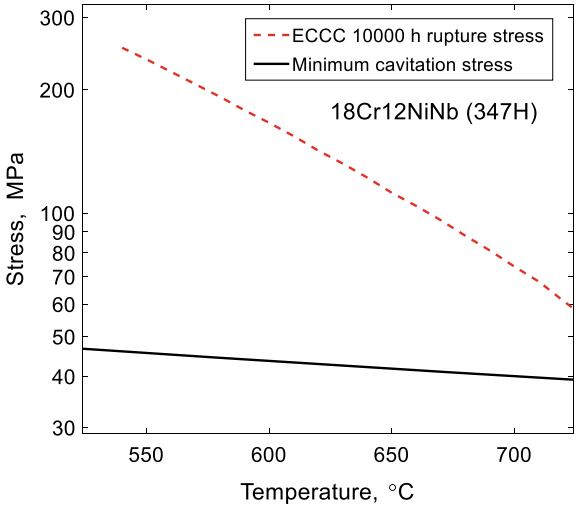

Fig. 10.2 Minimum cavitation stress versus temperature for TP347H austenitic stainless steel. 10000 h rupture data from ECCC for 347H are shown for comparison. Redrawn from [2] with permission of intechopen

10.4.2 Strain Dependence

Most researchers today assume that the nucleation of cavities is due to grain boundary sliding (GBS). There are several reasons for this. In many materials cavities are formed around particles in the grain boundaries. It has often been found experimentally that the number of cavities is proportional to the creep strain, Eq. (10.1). In addition, the amount of GBS is also proportional to the creep strain, Eq. (9.11)

$$u_{\mathrm{GBS}} = C_{\mathrm{s}}\varepsilon \tag{10.5}$$

The constant C_{s} is given by, Eq. (9.12)

$$C_{\mathrm{s}} = \dot{u}_{\mathrm{GBS}}/\dot{\varepsilon} = \frac{3\phi}{2\xi} d_{\mathrm{g}} \tag{10.6}$$

where d_{g} is the grain size, ϕ and ξ are constants.

To explain the experimental observations that the nucleation rate is proportional to the creep strain rate, Eq. (10.1), Sandström and Wu proposed the so called *double ledge model* [30]. Following the ideas in Lim's model [25], nucleation is assumed to take place when a subboundary on one side of a sliding grain boundary meets another subboundary on the opposite side. The position where a subboundary meets a grain boundary is referred to as a subgrain corner. The nucleation rate then takes the form

$$\frac{dn_{\mathrm{cav}}}{dt} = \frac{\dot{u}_{\mathrm{GBS}}}{d_{\mathrm{sub}}} \frac{1}{d_{\mathrm{sub}}^2} \tag{10.7}$$

where d_{sub} is the subgrain diameter. d_{sub} is inversely proportional to the dislocation stress that is in general close to the applied stress, Eq. (8.4). Equation (10.7) gives the nucleation rate per unit grain boundary area. It must also be added to Eq. (10.7) that at most one nucleus is formed in each subgrain. Equation (10.7) describes the situation for a particle free material. If particles are present, nucleation is assumed to occur when a subboundary hits a particle on a sliding grain boundary. Considering the nucleation at both particles and subgrain corners, the nucleation rate can be expressed as [31]

$$\frac{dn_{cav}}{dt} = \frac{0.9C_s}{d_{sub}}\left(\frac{g_{sub}}{d_{sub}^2} + \frac{g_{part}}{\lambda^2}\right)\dot{\varepsilon} = B_s\dot{\varepsilon} \tag{10.8}$$

where λ is the interparticle spacing in the grain boundary. In Eq. (10.8), factors g_{sub} and g_{part} are introduced for the fraction of subgrain corners and particles where cavity nucleation takes place. The values of g_{sub} and g_{part} will be discussed below. 0.9 is a factor that takes into account the averaging of different orientation. The derivation is comparatively lengthy. For this reason the derivation is not presented here [31].

10.4.3 Comparison to Experiments for Copper

Das et al. have recently presented measurements on nucleation of creep cavities in copper using small angle neutron scattering (SANS) [32]. Their results will be compared with the model in Sect. 10.4.2. They give values for the spacing λ_{cav} between cavities in the grain boundaries. The spacing can be transferred to the number of cavities n_{cav} per unit grain boundary area as

$$n_{cav} = 1/\lambda_{cav}^2 \tag{10.9}$$

The results for n_{cav} as a function of stress is shown in Fig. 10.3.

In Fig. 10.3 the model values are about a factor of 4 below the experimental ones but show the same stress dependence. The ratio between the tests at the two times is about the same. There is also another way to determine the cavity density in [32] from their volume fraction f_V and the cavity radii R_{cav}

$$n_{cav} = \frac{f_V}{\pi R_{cav}^2} \tag{10.10}$$

The values from Eq. (10.10) fall below the model values contrary to the values according to Eq. (10.9). Since it is more difficult to measure the volume fraction and the cavity radius than the cavity spacing, the values from Eq. (10.10) are more uncertain and are not shown in Fig. 10.3.

Das el al. evaluated the parameter B_s in Eq. (10.8), i.e. the ratio between the nucleation rate and the creep rate or expressed in another way the ratio between the

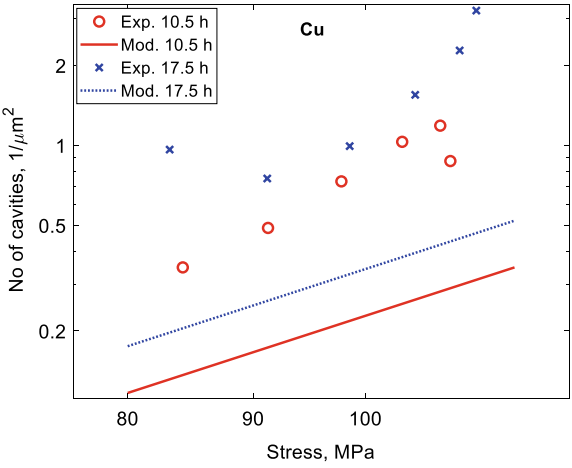

Fig. 10.3 Modeling and experimental number of cavities per unit grain boundary area as a function of stress for two testing times. Model values from Eq. (10.8) and experiments from [32]

cavity density and the creep strain. The experimental and the model values are given in Fig. 10.4. Unfortunately data are not available for exactly the testing time as in Fig. 10.3.

The model values are a factor of 2 above the experimental data this time. The stress dependence is about the same in the model and the experiments. It should be noticed that with the same model in the Figures, model values are above the experimental ones in Fig. 10.4 contrary to those in Fig. 10.3. This indicates an uncertainty in the experimental data and the consistency between models and observations is acceptable considering this effect. It is valuable that the fairly dramatic stress dependence in the model (σ^3) is reproduced in the observations.

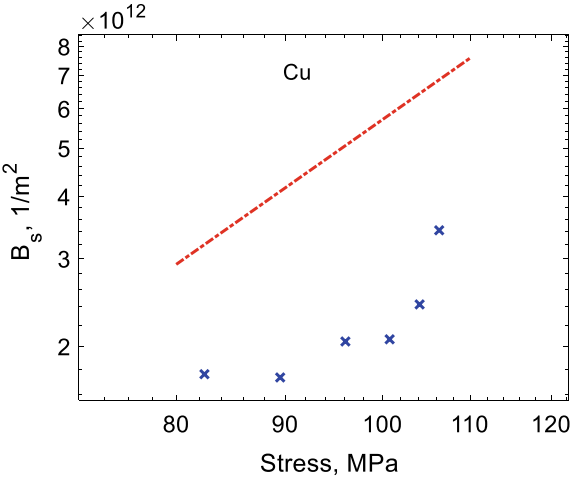

Fig. 10.4 Modeling and experimental values for the ratio B_s between the number of cavities per unit grain boundary area and the creep strain as a function of stress for a testing time of 17.5 h. Model values (line) from Eq. (10.8) and experiments (points) from [32]

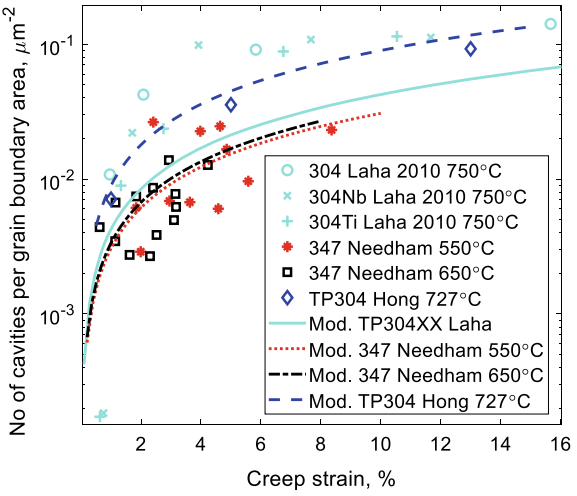

Fig. 10.5 Modeling and experimental number of cavities per unit grain boundary area as a function of creep strain for austenitic stainless steel collected from literature. Redrawn from [31] with permission of Springer

10.4.4 Comparison to Experiment for Austenitic Stainless Steels

A comparison of the model in Eq. (10.8) to experimental data for austenitic stainless is given in Fig. 10.5. Data for TP347 (17Cr12NiNb), TP304 (18Cr10Ni) and TP321 (17Cr10NiTi) are presented. Nucleation at both subgrain corners and particles are taken into account. Considering the scatter in the data, the observations give good support to the model. In Fig. 10.5, the factors g_{sub} and g_{part} are taken as unity. Thus every subgrain corner and particle is assumed to contribute to the nucleation. This cannot always be assumed to be the case but systematic studies have not been found.

10.5 Models for Cavity Growth

10.5.1 Unconstrained Cavity Growth Model

Once the cavities have been nucleated they can start to grow if they exceed a critical size. Growth of creep cavities are in general assumed to be controlled by diffusion. There can also be contributions from straining. Strain controlled growth is considered in Sect. 10.5.3. A diffusion controlled growth model was first proposed by Hull and Rimmer [13]. Beere and Speight simplified this formulation [33] and this is the version that is used nowadays

$$\frac{dR_{\text{cav}}}{dt} = 2D_0K_{\text{f}}(\sigma - \sigma_0)\frac{1}{R_{\text{cav}}^2} \tag{10.11}$$

R_{cav} is the cavity radius in the grain boundary plane, dR_{cav}/dt its growth rate, σ the applied stress, σ_0 the sintering stress $2\gamma_s \sin(\alpha)/R_{cav}$, where γ_s is the surface energy of the cavity per unit area and α the cavity tip angle. The presence of the sintering stress σ_0 ensures that only cavities that are larger than a critical size grow. δ the grain boundary width, D_{GB} the grain boundary self-diffusion coefficient, Ω the atomic volume are combined into a grain boundary diffusion parameter D_0, $D_0 = \delta D_{GB}\Omega/k_B T$. k_B is the Boltzmann's constant and T the absolute temperature. The factor K_f was introduced in [34]. It takes into account the role of the size of the cavity in relation to that of the surrounding area that can deliver vacancies for the growth of the cavity. It is a function of the cavitated grain boundary area fraction $f_a = (2R/\lambda_{cav})^2$

$$K_f = -1/\left[2\log f_a + (1 - f_a)(3 - f_a)\right] \tag{10.12}$$

λ_{cav} is the spacing between cavities in the grain boundary. It can be determined from number of cavities per unit grain boundary area n_{cav}, cf. Eq. (10.9)

$$\lambda_{cav} = 1/\sqrt{n_{cav}} \tag{10.13}$$

n_{cav} is derived with the nucleation relation, Eq. (10.8).

The cavities cannot grow unless the stress is larger than the sintering stress σ_0. This means that the cavity radius must have reached a certain size for growth to take place, which is referred to as the nucleation radius R_{nucl}. From the expression for the sintering stress, R_{nucl} can be found

$$R_{nucl} = \frac{2\gamma_s \sin(\alpha)}{\sigma} \tag{10.14}$$

Das et al. give data for the cavity radius for short creep testing times measured with small angle neutron scattering (SANS) [32]. The cavity radii should be close to R_{nucl}. A comparison between their data and Eq. (10.14) is illustrated in Fig. 10.6.

In Fig. 10.6, a cavity tip angle of 55° has been assumed. A precise value of the tip angle is not known but in the literature values of 50–70° are often used. It can be seen that the nucleation radius is well represented by Eq. (10.14). The mechanisms for the initial growth of creep cavities are not well established. But it is likely that it takes place by GBS, see Sect. 10.5.4. Since the cavities are initiated by GBS, it is reasonable that the first growth also occurs by this mechanism.

10.5.2 Constrained Cavity Growth

It was early on found that the expression for diffusion growth in Eq. (10.11) often exceeded observed values. Dyson noticed that the predicted growth rate many times was larger than the creep strain rate which he considered to be unphysical [9]. He

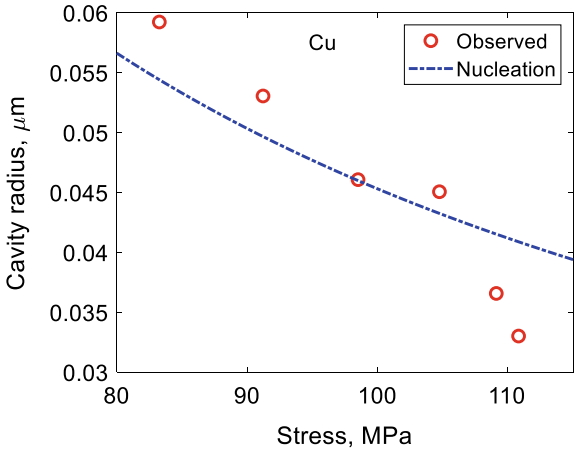

Fig. 10.6 Modeling and experimental values for the cavity nucleation radius as a function of stress for the testing time 17.5 h for Cu. Model values from Eq. (10.14) and experiments from [32]

suggested that the growth rate should always be less than the creep rate that is referred to as *constrained growth*. Here the expression for constrained growth derived by Rice will be used [14]

$$\frac{dR_{\text{cav}}}{dt} = 2D_0K_{\text{f}}(\sigma_{\text{red}} - \sigma_0)\frac{1}{R_{\text{cav}}^2} \tag{10.15}$$

The only difference between Eqs. (10.11) and (10.15) is that the applied stress is replaced by a reduced stress σ_{red}

$$\sigma_{\text{red}} = \sigma_0 + \frac{1}{\frac{1}{\sigma} + \frac{32D_0K_{\text{f}}}{\lambda_{\text{cav}}^2 d_{\text{g}}\beta\dot{\varepsilon}(\sigma)}} \tag{10.16}$$

where β is a material constant (β = 1.8 for homogeneous materials), and d_{g} the grain diameter. Equation (10.15) satisfies the criterion formulated by Dyson.

In Rice's paper an assumption was made about linear viscoplastic opening of a crack. In a reanalysis, He and Sandström did not make the assumption about linearity [35]. A grain structure with a pillar of height h and width corresponding to the grain size d_{g} was set up. The creep deformation in this pillar in the loading direction z can be expressed as

$$\frac{dz}{dt} = 4\pi D_0K_{\text{f}}(\sigma_{\text{red}} - \sigma_0)n_{\text{cav}} + h\dot{\varepsilon}(\sigma_{\text{red}}) = h\dot{\varepsilon}(\sigma) \tag{10.17}$$

$\dot{\varepsilon}(\sigma_{\text{red}})$ and $\dot{\varepsilon}(\sigma)$ are the creep rates at the reduced and applied stress, respectively. In the first expression for $\frac{dz}{dt}$ the first term is the volume growth rate of a cavity multiplied by the number of cavities per unit grain boundary area. The second term is the creep displacement of the pillar at the reduced stress. The second expression for $\frac{dz}{dt}$ is the displacement of the surrounding material at the applied stress. According

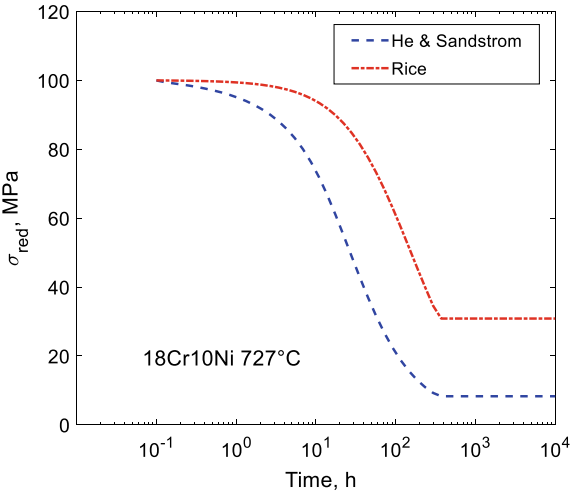

Fig. 10.7 Reduced stresses according to Eq. (10.16) (dash-dotted) and (10.18) (dashed) versus time for the austenitic stainless steel 18Cr10 Ni (TP304) at 727 °C and 100 MPa. Redrawn from [36] with permission of Elsevier

to Eq. (10.17), the cavity growth rate plus the creep rate around the cavity matches the average creep rate. This is a stronger criterion than the original requirement on constraint. The height of the pillar h was determined with finite element analysis. The finding was that the pillar height was related to the cavity radius $h \approx 2R_{\text{cav}}$ [35]. With this result, Eq. (10.17) takes the form

$$2\pi D_0 K_{\text{f}}(\sigma_{\text{red}} - \sigma_0)/L^2 R_{\text{cav}} + \dot{\varepsilon}(\sigma_{\text{red}}) = \dot{\varepsilon}(\sigma) \tag{10.18}$$

To find σ_{red}, the equation has to be solved by iteration. This new value for σ_{red} is lower than what the expression (10.16) gives. An illustration of this is presented in Fig. 10.7. In particular, the difference is significant at longer times.

These reduced stresses are quite important when describing experimental data. A comparison to experimental data for common austenitic stainless steel is shown in Fig. 10.8. Data for 18Cr10Ni steel with and without Nb or Ti are illustrated. This new model for constrained growth clearly gives an improved description of data.

10.5.3 Strain Controlled Cavity Growth

A contribution from plastic deformation to cavity growth can also be obtained. The most well established model is due to Cocks and Ashby [37]. They analyze how the area fraction f_{h} of cavities in a grain boundary perpendicular to the loading direction increases with strain. They derived the following time derivatives for f_{h} and the axial strain ε_{a} in the loading direction

$$\frac{df_{\text{h}}}{dt} = \frac{\dot{\varepsilon}_{\text{ss}}}{\alpha_h}\left\{\frac{1}{(1-f_{\text{h}})^{n_{\text{N}}}} - (1-f_{\text{h}})\right\} \tag{10.19}$$

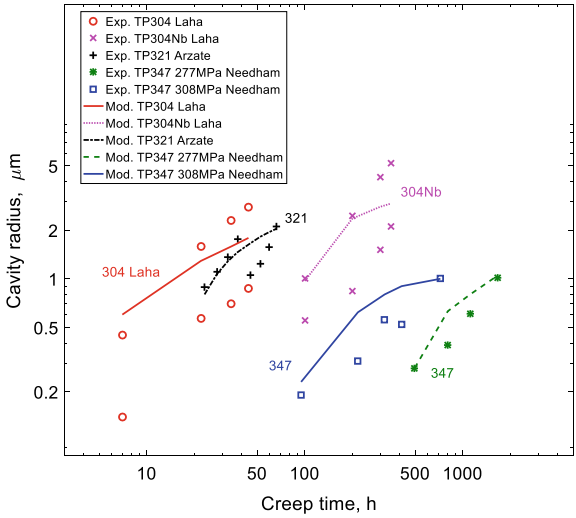

Fig. 10.8 Cavity radius as a function of creep time for 18Cr10Ni without or with Nb (347) or Ti (321) austenitic stainless steels. The creep tests were performed at temperatures in the interval of 650–812 °C. Redrawn from [36] with permission of Elsevier

$$\frac{d\varepsilon_a}{dt} = \dot{\varepsilon}_{ss}\left\{1 + \frac{2R_h}{\alpha_h d_g}\left(\frac{1}{(1-f_h)^{n_N}} - (1-f_h)\right)\right\} \tag{10.20}$$

where the stationary creep is given by

$$\dot{\varepsilon}_{ss} = \dot{\varepsilon}_0\left(\frac{\sigma_e}{\sigma_0}\right)^{n_N} \tag{10.21}$$

and

$$\alpha_h = 1/\sinh\left\{\frac{(n_N - 1/2)}{(n_N + 1/2)}\frac{\sigma_h}{\sigma_e}\right\} \tag{10.22}$$

R_h is the initial cavity radius, d_g the grain size, σ_e the effective stress and σ_h the hydrostatic stress. $\dot{\varepsilon}_0$, σ_0, and n_N are constants describing the creep rate. By integrating Eqs. (10.19) and (10.20) the cavitated area fraction can be obtained. An example is shown in Fig. 10.9. An initial cavitated area fraction of 0.001 is assumed.

The increase in cavitated area fraction is much larger if a larger initial value is assumed, which does not seem to be realistic. If the plastic growth is combined with diffusion growth, significant contributions can be obtained. The problem with the model is that it is not consistent with the principle of constrained growth. The strain rate around the cavities can become many times larger than the average creep rate and that should not be the situation during constrained growth. This effect is however small for low cavitated area fractions, so the results in Fig. 10.9 are still valid.

Describing the growth rate due to plastic deformation can be handled with a model that has been developed by Danavas and Solomon [38]

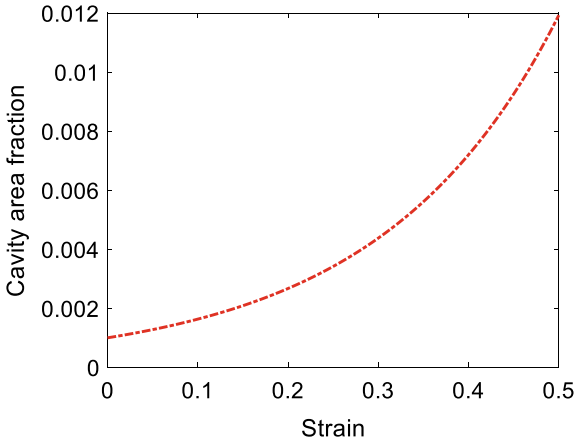

Fig. 10.9 Cavitated area fraction in grain boundary as a function of strain according to Eqs. (10.19) and (10.20). Creep exponent $n_N = 7$

$$\frac{dR_{cav}}{dt} = \frac{\sin^2(\alpha_{tip})}{\alpha_{tip} - \sin(\alpha_{tip})\cos(\alpha_{tip})} \exp\left(\frac{3\sigma_H}{2\sigma_e} - \frac{1}{2}\right) \frac{R_{cav}}{3} \dot{\varepsilon}(\sigma_{red}) \tag{10.23}$$

where α_{tip} is the tip angle of the cavity. An important modification has been made in Eq. (10.23) in comparison to the original model in [38]. The creep rate is computed for the reduced stress, not for the applied stress to make it consistent with Eq. (10.18). The expression gives a modest increase in the cavity size except if multiaxial stress states are taken into account. In Eq. (10.23) this is considered with the help of an expression from Rice and Tracey [39]. There are several alternative ways that have been proposed for the influence of multiaxial stress state derived from cavity growth during ductile fracture. The role of multiaxial stress cannot be considered to be fully settled.

10.5.4 Growth Due to Grain Boundary Sliding

It is well established that cavities are often elongated in the plane of the grain boundary. As has been analyzed in detail above, it is natural to assume that cavities are nucleated due to grain boundary sliding (GBS). Once the cavities have been nucleated for example around particles, the cavities will be exposed to shearing due to the continuing GBS. It is possible that some cavities expand at the same rate as the GBS. From Eq. (10.5) this will give a cavity size of

$$R_{cav} = C_s \varepsilon \tag{10.24}$$

where C_s is again given by Eq. (10.6), This expression is compared with data for a 12CrMo steel and a TP347 (17Cr12NiNb) austenitic stainless steel in Fig. 10.10.

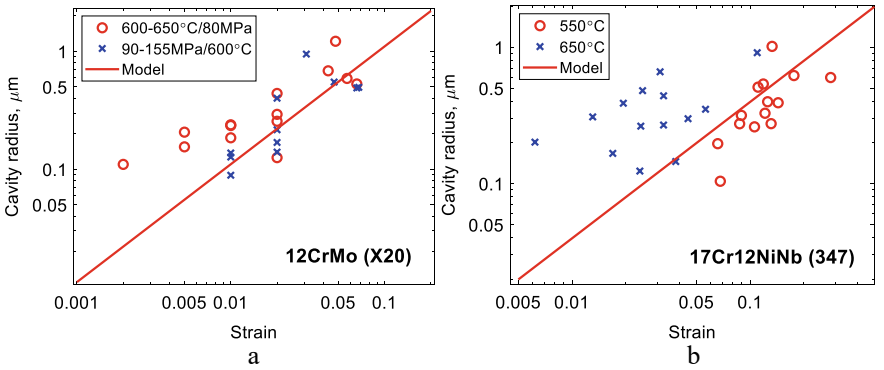

Fig. 10.10 Cavity radius versus strain. Model according Eq. (10.24); **a** 12CrMo steel (X20). Data from [40]; **b** TP347 (17Cr12NiNb). Data from [41]. **b** Redrawn from [42] with permission of Taylor & Francis

The results give a reasonable description of the cavity growth data for the two steels. The amount of data to make comparisons to the model is limited. Since the constant C_s is proportional to the grain size, the model predicts large cavity radii when the grain size is large, which might not be realistic.

10.6 Summary

- Nucleation of creep cavities is assumed to take place at particles and subboundary junctions in the grain boundaries by grain boundary sliding (GBS). This assumption makes it possible to quantitatively explain the observed strain dependence of the number of cavities. In the past attempts have been made to use classical nucleation theory, but it gives essentially a step function in stress that is in direct variance with observations.
- Diffusion controlled growth of cavities can satisfactorily describe observations for austenitic stainless steels if recent modeling for constrained growth is taken into account. Constrained growth ensures that the cavities are not expanding faster than the creep rate of the matrix.
- Several expressions for strain controlled growth exist that are derived from basic physical principles. However, these expressions are difficult to verify experimentally since the starting cavity size has a significant effect on the result and there is no well-defined way of choosing the size. In addition, some expressions do not fulfil the requirements on constrained growth which can give overestimated growth rates. A recent model based on GBS avoids these difficulties. The model reproduces the limited experimental data that are available.

References

1. M.E. Kassner, T.A. Hayes, Creep cavitation in metals. Int. J. Plast. **19**, 1715–1748 (2003)
2. R. Sandström, J. He, Survey of creep cavitation in fcc metals, in *Study of Grain Boundary Character* (inTech, 2017), pp. 19–42
3. R. Raj, M.F. Ashby, Intergranular fracture at elevated temperature. Acta Metall. **23**, 653–666 (1975)
4. B.F. Dyson, Continuous cavity nucleation and creep fracture. Scr. Metall. **17**, 31–37 (1983)
5. R. Wu, R. Sandstrom, Strain dependence of creep cavity nucleation in low alloy and 12%Cr steels. Mater. Sci. Technol. Ser. **12**, 405–415 (1996)
6. M.H. Yoo, H. Trinkaus, Crack and cavity nucleation at interfaces during creep. Metall. Trans. A Phys. Metall. Mater. Sci. **14 A**, 547–561 (1982)
7. H. Riedel, Cavity nucleation at particles on sliding grain boundaries. A shear crack model for grain boundary sliding in creeping polycrystals. Acta Metall. **32**, 313–321 (1984)
8. L.C. Lim, H.H. Lu, Effect of substructure on intergranular cavitation at high temperature. Scripta Metall. Mater. **31**, 723–728 (1994)
9. B.F. Dyson, Constraints on diffusional cavity growth rates. Metal Sci. **10**, 349–353 (1976)
10. Q. Meng, Z. Wang, Creep damage models and their applications for crack growth analysis in pipes: a review. Eng. Fract. Mech. **205**, 547–576 (2019)
11. B. Neubauer, F. Arens-Fischer, Determination of residual life of power station components subject to creep stress. VGB-Kraftwerkstechnik **63**, 637–645 (1983)
12. G. Sposito, C. Ward, P. Cawley, P.B. Nagy, C. Scruby, A review of non-destructive techniques for the detection of creep damage in power plant steels. NDT E Int. **43**, 555–567 (2010)
13. D. Hull, D.E. Rimmer, The growth of grain-boundary voids under stress. Philos. Mag. **4**, 673–687 (1959)
14. J.R. Rice, Constraints on the diffusive cavitation of isolated grain boundary facets in creeping polycrystals. Acta Metall. **29**, 675–681 (1981)
15. A.M. Othman, B.F. Dyson, D.R. Hayhurst, J. Lin, Continuum damage mechanics modelling of circumferentially notched tension bars undergoing tertiary creep with physically-based constitutive equations. Acta Metall. Mater. **42**, 597–611 (1994)
16. Z.L. Kowalewski, D.R. Hayhurst, B.F. Dyson, Mechanisms-based creep constitutive equations for an aluminium alloy. J. Strain Anal. Eng. Des. **29**, 309–316 (1994)
17. I.J. Perrin, D.R. Hayhurst, Creep constitutive equations for a 0.5Cr–0.5Mo–0.25V ferritic steel in the temperature range 600–675 °C. J. Strain Anal. Eng. Des. **31**, 299–314 (1996)
18. B.J. Cane, Creep fracture of dispersion strengthened low alloy ferritic steels. Acta Metall. **29**, 1581–1591 (1981)
19. J.A. Siefert, J.D. Parker, Evaluation of the creep cavitation behavior in Grade 91 steels. Int. J. Pres. Ves. Pip. **138**, 31–44 (2016)
20. E. Smith, J.T. Barnby, Crack nucleation in crystalline solids. Metal Sci. J. **1**, 56–64 (1967)
21. R. Raj, Nucleation of cavities at second phase particles in grain boundaries. Acta Metall. **26**, 995–1006 (1978)
22. H. Riedel, Life prediction methods for constrained grain boundary cavitation. Int. J. Pres. Ves. Pip. **39**, 119–134 (1989)
23. X.G. Jiang, J.C. Earthman, F.A. Mohamed, Cavitation and cavity-induced fracture during superplastic deformation. J. Mater. Sci. **29**, 5499–5514 (1994)
24. T.G. Langdon, The role of grain boundaries in high temperature deformation. Mater. Sci. Eng. A **166**, 67–79 (1993)
25. L.C. Lim, Cavity nucleation at high temperatures involving pile-ups of grain boundary dislocations. Acta Metall. **35**, 1663–1673 (1987)
26. J. He, R. Sandström, Modelling grain boundary sliding during creep of austenitic stainless steels. J. Mater. Sci. **51**, 2926–2934 (2016)
27. R. Wu, J. Hagstrom, R. Sandstrom, Grain boundary sliding in phosphorus alloyed oxygen-free copper under creep, Swedish Nuclear Waste Management Company Report R-15-14 (2015)

28. R. Sandström, R. Wu, J. Hagström, Grain boundary sliding in copper and its relation to cavity formation during creep. Mater. Sci. Eng. A **651**, 259–268 (2016)
29. P.J. Henderson, R. Sandstrom, Low temperature creep ductility of OFHC copper. Mater. Sci. Eng. A **246**, 143–150 (1998)
30. R. Sandström, R. Wu, Influence of phosphorus on the creep ductility of copper. J. Nucl. Mater. **441**, 364–371 (2013)
31. J. He, R. Sandström, Formation of creep cavities in austenitic stainless steels. J. Mater. Sci. **51**, 6674–6685 (2016)
32. Y. Das, A. Fernandez-Caballero, E. Elmukashfi, H. Jazaeri, A. Forsey, M.T. Hutchings, R. Schweins, P.J. Bouchard, Stress driven creep deformation and cavitation damage in pure copper. Mater. Sci. Eng.: A **833** (2021)
33. M.V. Speight, W. Beere, Vacancy potential and void growth on grain boundaries. Metal Sci. J. **9**, 190–191 (1975)
34. W. Beere, M.V. Speight, Creep cavitation by vacancy diffusion in plastically deforming solid. Metal Sci. **21**, 172–176 (1978)
35. J. He, R. Sandström, Growth of creep cavities in austenitic stainless steels, in *8th European Stainless Steel & Duplex Stainless Steel Conference, ASMET* (2015), pp. 561–570
36. J. He, R. Sandström, Creep cavity growth models for austenitic stainless steels. Mater. Sci. Eng. A **674**, 328–334 (2016)
37. A.C.F. Cocks, M.F. Ashby, Intergranular fracture during power-law creep under multiaxial stresses. Metal Sci. **14**, 395–402 (1980)
38. K. Davanas, A.A. Solomon, Theory of intergranular creep cavity nucleation, growth and interaction. Acta Metall. Mater. **38**, 1905–1916 (1990)
39. J.R. Rice, D.M. Tracey, On the ductile enlargement of voids in triaxial stress fields*. J. Mech. Phys. Solids **17**, 201–217 (1969)
40. R. Wu, R. Sandstrom, Creep cavity nucleation and growth in 12Cr–Mo–V Steel. Mater. Sci. Technol. Ser. **11**, 579–588 (1995)
41. N.G. Needham, T. Gladman, Nucleation and growth of creep cavities in a type 347 steel. Metal Sci. **14**, 64–72 (1980)
42. R. Sandström, J.-J. He, Prediction of creep ductility for austenitic stainless steels and copper. Mater. High Temp. **39**(6), 427–435 (2022)